8 Time Dependence of Fluorescence Anisotropy

8.1 Introduction

Time-resolved fluorescence depolarization studies have, since the early 1970s, provided an interesting method for monitoring molecular reorientational motions in solution. Until recently the relatively poor quality of much of the data available from these measurements has precluded detailed quantitative interpretations of the results. With the advent of improved experimental techniques for fluorescence decay time determinations interest in the technique has been revived.

When an ensemble of fluorescent chromophores is illuminated an anisotropy will be created in the system since only those species with a component of the absorption transition moment in the same direction as the polarization vector of the incident light will be excited. When plane-polarized excitation radiation is employed, if the fluorescence emission transition moment maintains a fixed geometrical relationship with that for the absorption process, steady-state illumination leads to three distinct cases.

8.1.1 Steady-state anisotropy measurements

The Perrin equation (8.1) relates anisotropy r (Equation 8.2) to initial anisotropy r_0, the fluorescence decay time τ_F and the rotational relaxation time, τ_r.

$$\frac{1}{r} = \frac{1}{r_0}\left[1 + \frac{3\tau_F}{\tau_r}\right] \tag{8.1}$$

$$r = \frac{(I_{||} - I_{\perp})}{(I_{||} + 2I_{\perp})} \tag{8.2}$$

Here $I_{||}$ and $I_{\perp}$ are the fluorescence intensity components parallel and perpendicular to the plane of polarization of the electric vector of the incident radiation. The three possible cases are as follows:

(A) If $\tau_F \ll \tau_r$ then $r \approx r_0$ and τ_r is difficult to measure (the fluorescence decays before the molecule moves).

(B) If $\tau_F \gg \tau_r$ then $r=0$ and the anisotropy (and thus τ_r) cannot be accurately measured.

(C) If $\tau_F \approx \tau_r$ This represents the best case for accurate determination of $\tau_r (0 < r < r_0)$.

For conventional emitting species with fluorescence decay times of the order of ns, rotational motion must be restricted if it is to occur on this timescale. This can be achieved in small molecules by use of viscous solvents, or by incorporating the chromophore into a macromolecule of synthetic or biological origin. Effects resulting from the use of unpolarized exciting radiation will be discussed later.

8.1.2 Time-resolved anisotropy measurements

Spencer and Weber (1969) have derived the relevant equations for the time dependence of $I_{||}$ (Equation 8.3) and $I_\perp$ (Equation 8.4), for single τ_r

$$I_{||}(t) = e^{-t/\tau_F}(1 + 2r_0 e^{-t/\tau_r}) \tag{8.3}$$

$$I_\perp(t) = e^{-t/\tau_F}(1 - r_0 e^{-t/\tau_r}) \tag{8.4}$$

The total fluorescence intensity $F(t)$ is given by Equation 8.5:

$$\begin{aligned} F(t) &= I_{||}(t) + 2I_\perp(t) \\ &= 3e^{-t/\tau_F} \\ &= F_0 e^{-t/\tau_F} \end{aligned} \tag{8.5}$$

and the time dependent anisotropy, $r(t)$ is given by:

$$\begin{aligned} r(t) &= [I_{||}(t) - I_\perp(t)/(I_{||}(t) + 2I_\perp(t)] \\ &= r_0 e^{-t/\tau_r} \end{aligned} \tag{8.6}$$

$F(t)$ depends upon τ_F, and $r(t)$ only upon τ_r, so that these two lifetimes can be separated. This separation is not possible in steady state measurements. (The degree of polarization, P, defined as $(I_{||} - I_\perp)/(I_{||} + I_\perp)$, is not independent of τ_F and is therefore not as useful a quantity as r). Again three limiting cases can be considered.

(a) If $\tau_F < \tau_r$, the fluorescence decays before the anisotropy decays, and hence only r_0 can be measured.

(b) If $\tau_r < \tau_F$, in contrast to steady-state measurements, τ_r can be measured in principle, for as Fig. 8.1 shows, the *decay* of the parallel and perpendicular components depends only upon τ_r. The one experimental disadvantage of this case is that

those photons emitted after the period of a few times τ_r cannot contribute toward the determination of τ_r, but provided the signal-to-noise ratio is favourable, this need not be of great concern. However, there *can* be conditions in which the signal-to-noise ratio is unfavourable due to the experimental limitations dictated by the need to avoid pulse pile-up. While it is always disadvantageous to use a fluorophore with $\tau_r \gg \tau_F$ for measurement of τ_r [case (a)], one of the advantages of time-resolved anisotropy measurements lies in being able to extend the time range over which a given fluorophore can be used for accurate measurement of τ_r.

(c) $\tau_r \approx \tau_F$. This is the ideal experimental situation since almost all photons are counted within the time (equal to several rotational relaxation times) in which $r(t)$ shows measurable changes.

8.2 Effects of Polarization on Intensity Measurements

8.2.1 Instrument response

Before discussing methods of measuring time-dependent anisotropy of fluorescence, we emphasize that polarization effects can be of importance in

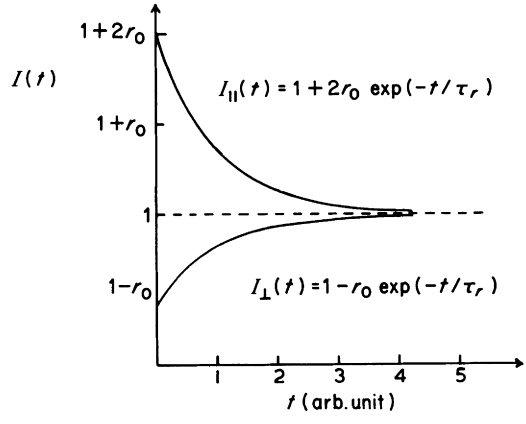

Figure 8.1 Idealized representation of the decay of $I_{\parallel}(t)$ and $I_{\perp}(t)$ when $\tau_r < \tau_F$. τ_r assumed to be equal to 1 time unit.

all fluorescence intensity, including conventional decay time, measurements. We must first recognize that the instrument monitoring the fluorescence, particularly the spectral dispersion element, responds differently to different polarizations of light, thus occasioning a need for a correction factor. For example, the use of diffraction gratings can yield intensities of emission which depend strongly upon orientation with respect to the plane of the grating. It is inevitably necessary when using such instruments to correct for the anisotropy in response. This instrumental anisotropy is usually termed the G factor and is defined as the ratio of the transmission efficiency for vertically polarized light to the transmission efficiency for horizontally polarized light. If in the simple instrument shown in Fig. 8.2, the two planes of exciting radiation, horizontal, H, and vertical, V, are as defined in the diagram with respect to the planes of observation of fluorescence, $I_{||}$ and $I_{\perp}$, then for horizontally polarized exciting radiation, $I_{||}$ and $I_{\perp}$ should be identical, or $(I_{||}/I_{\perp})_{H}=1$. If measured values of $G[=(I_{||}/I_{\perp})_{H}]$ deviate from unity, a correction factor must be applied to all measurements of $I_{||}$ and $I_{\perp}$ excited with vertically polarized light, $(I_{||}/I_{\perp})_{V}$. Thus

$$\frac{(I_{||})}{(I_{\perp})_{\text{V corrected}}}=\frac{(I_{||})}{(I_{\perp})_{V}}\Big/\frac{(I_{||})}{(I_{\perp})_{H}}. \tag{8.7}$$

Hence values of fluorescence anisotropy, r, corrected for instrumental response, would be given by:

$$r=\frac{(I_{||}/I_{\perp})-G}{(I_{||}/I_{\perp})+2G}. \tag{8.8}$$

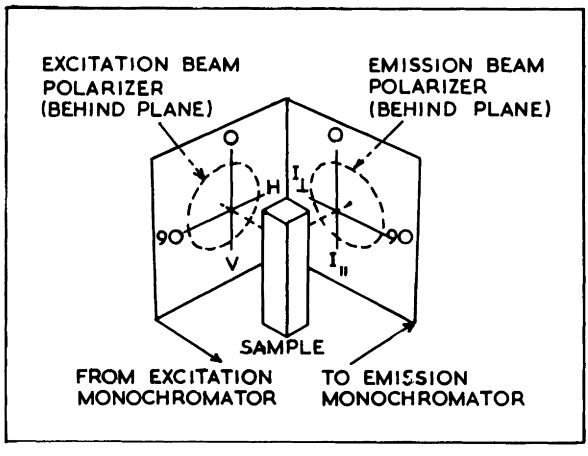

Figure 8.2 Representation of planes of polarization of incident and fluorescent light.

8.2.2 Elimination of polarization bias in intensity measurements

The removal of unwanted effects of photoselection (preferential excitation of molecules with specific orientations with respect to excitation radiation, both polarized and unpolarized) has been discussed thoroughly by Mielenz *et al.* (1976), from whom we have paraphrased the following analysis. The general case for steady-state illumination is illustrated in Fig. 8.3, in which the exciting radiation is assumed to be *partially* polarized, and is regarded as an incoherent superposition of two plane polarized components S^V and S^H having orthogonal electric field vectors, E^V and E^H. The intensity of the fluorescence emission is detected at an arbitrary viewing direction α in the horizontal plane, and is resolved into four components with electric field vectors E_V^V, E_V^H, E_H^V, and E_H^H where superscripts denote state of polarization of exciting radiation, and subscripts that of fluorescence.

The intensities of these four components are

$$I_V^V(\alpha) = (E_V^V)^2 = 1/3kS^V\tau(1+2r) \tag{8.9}$$

$$I_V^H(\alpha) = (E_V^H)^2 = 1/3kS^H\tau(1-r) \tag{8.10}$$

$$I_H^V(\alpha) = (E_H^V)^2 = 1/3kS^V\tau(1-r) \tag{8.11}$$

$$I_H^H(\alpha) = (E_H^H)^2 = 1/3kS^H\tau(1-r+3\cos^2\alpha) \tag{8.12}$$

k is a proportionality factor, τ is the overall molecular cross-section for

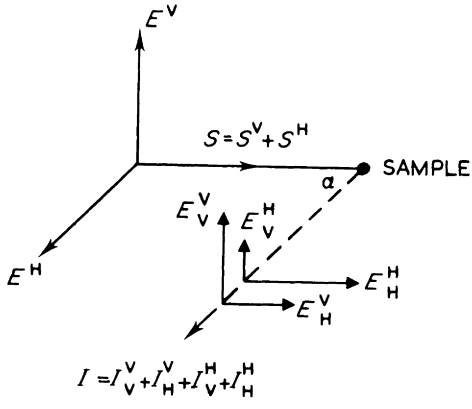

Figure 8.3 Excitation of a sample by partially polarized light composed of a superposition of two plane polarized components, S and S^H. E^V and E^H are the corresponding electric field vectors. For the other symbols see text (after Mielenz *et al.*, 1976).

fluorescence, and r is the emission anisotropy defined as in Equation 8.6, and also given by Equation 8.13 as

$$r = 1/5(3\cos^2\theta - 1), \tag{8.13}$$

where θ is the angle that the emission dipole has at the time of emission relative to the position of the absorption dipole at the moment of absorption.

There are several methods which can be used to obtain intensity measurements corrected for polarization

Method 1

The most cumbersome is to take readings, R, equivalent to Equations 8.9–8.12 using vertical and horizontal polarised excitation *and* emission.

These are then

$$R_V^V(\alpha) = I_V^V(\alpha)T_V \tag{8.14}$$

$$R_V^H(\alpha) = I_V^H(\alpha)T_V \tag{8.15}$$

$$R_H^V(\alpha) = I_H^V(\alpha)T_H \tag{8.16}$$

$$R_H^H(\alpha) = I_H^H(\alpha)T_H \tag{8.17}$$

where T_V and T_H are the response factors of the detection system (see above) for vertically and horizontally polarized light respectively. These raw data are then used to calculate the excitation (Equation 8.18) and emission (Equation 8.19) correction factors

$$F = S^V/S^H \tag{8.18}$$

$$G = T_V/T_H \tag{8.19}$$

and the emission dichroic ratio D, related to the emission anisotropy r, by Equation 8.20:

$$r = (D-1)/(D+2). \tag{8.20}$$

The information R_0, which would be obtained from an equivalent but depolarized sample is then

$$R_0 = 1/3k(S^V + S^H)(T_V + T_H)\tau \tag{8.21}$$

The procedure is informative, but unnecessarily time-consuming, particularly if R_0 is the only parameter required, and other alternatives are available.

Method 2 (Spencer and Weber, 1970)

This method was developed for *lifetime* measurements, τ_F, free from spurious effects of polarization, but is used for intensity measurements also. The

authors used *vertically* polarized exciting radiation, and right angle ($\alpha = 90$) viewing. The emission polarizer was set at an angle ϕ, (Fig. 8.4), and the total transmitted intensity when $\phi = \cos^{-1}(1/\sqrt{3}) = 54.75^0$ or 125.25^0, is given by Equation 8.22.

$$\begin{aligned} I_\phi^V(\alpha) &= (E_V^V \cos\phi)^2 + (E_H^V \sin\phi)^2 \\ &= 1/3 I_V^V(\alpha) + 2/3 I_H^V(\alpha) \end{aligned} \tag{8.22}$$

which is *independent* of r, and can be written as

$$I_\phi^V(\alpha) = 1/3 k S^V \tau \tag{8.23}$$

The responses T_V and T_H with respect to ϕ are given by

$$\begin{aligned} T_\phi &= T_V \cos^2\phi + T_H \sin^2\phi \\ &= 1/3(T_V + 2T_H) \\ &= 1/3\, T_H(G+2). \end{aligned} \tag{8.24}$$

The detector signal,

$$\begin{aligned} R_\phi^V(\alpha) &= T_\phi I_\phi^V(\alpha) \\ &= 1/9 k S^V T_H(G+2)\tau, \end{aligned} \tag{8.25}$$

is *also* independent of r, and therefore represents an *unbiased* measure of the fluorescence cross-section. *Hence the use of an emission polarizer at the so-called magic angle of 54.75° (or 125.25°) with vertically polarized exciting light eliminates bias due to polarization effects for all viewing angles, not just $\alpha = 90°$.*

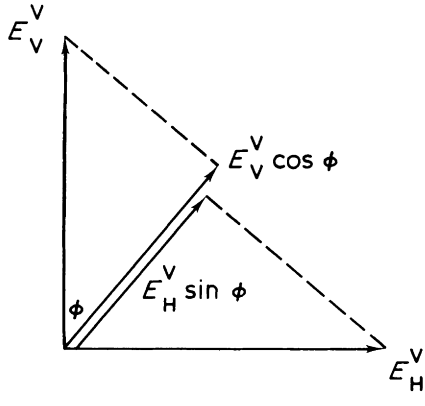

Figure 8.4 Electric field vector components of fluorescence intensity transmitted by a polarizer set at angle ϕ. Vertically polarized excitation (after Mielenz *et al.*, 1976).

Method 3

If the excitation radiation is *unpolarized* an unbiased detection signal can also be obtained if the same magic angle ϕ is used for the detector polarizer, but with α now specific. With no excitation polarizer, the emission detector signal will be

$$R_\phi(\alpha) = T_\phi T_\phi^{V}(\alpha) + I_\phi^{H}(\alpha), \tag{8.26}$$

where $I_\phi^{V}(\alpha)$ is as in Equation 8.23, and $I_\phi^{H}(\alpha)$, with reference to Fig. 8.5 is given by

$$\begin{aligned} I_\phi^{H}(\alpha) &= (E_V^{H} \cos\phi)^2 + (E_H^{H} \sin\phi)^2 \\ &= 1/3 I_V^{H}(\alpha) + 2/3 I_H^{H}(\alpha) \\ &= 1/3 k S^{H} \tau [1 - r(1 - 2\cos^2\alpha)]. \end{aligned} \tag{8.27}$$

The polarization bias of I^{H} will be removed if

$$\alpha = \cos^{-1}(1/\sqrt{2}) = 45^\circ \text{ or } 135^\circ, \tag{8.28}$$

so that $I_\phi^{H}(45) = 1/3 k S^{H} \tau$.

Hence

$$R_\phi(45) = 1/9 k (S^{V} + S^{H}) T_H (G + 2)\tau \tag{8.29}$$

and is also independent of r.

The main advantage of Method 3 is that there is no need for an excitation polarizer. Furthermore, only one measurement is required. The disadvantage is that the technique is very sensitive to angular misalignment. For $\alpha = 90^\circ$ and emission polarizer set at vertical or horizontal (Method 1), the first derivatives of the detector response with respect to α and ϕ are zero, whereas for the arrangements in Method 3, this is not so, and misalignment affects $R_\phi(45)$.

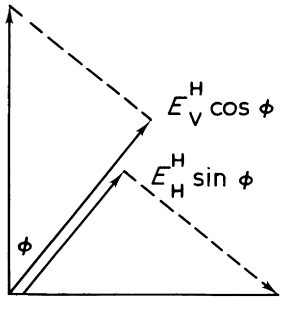

Figure 8.5 Electric field vector components of fluorescence intensity transmitted by a polarizer set at angle ϕ. Horizontally polarized excitation (after Mielenz *et al.*, 1976).

Method 4 (Spencer and Weber, 1970)

Here no excitation polarizer is used, the emission polarizer is set at $\phi = \cos^{-1}(2/3)^{1/2}$, (35.25°) and right-angle viewing ($\alpha = 90°$) is used. In this case, it can be shown (Mielenz *et al.*, 1976) that

$$\begin{aligned} R_\phi(90) &= T_\phi[2/3I_V^V(90) + I_V^H(90) + 1/3I_H^V(90) + I_H^H(90)] \\ &= 1/3kS^H T_\phi \tau(F+1) + r(F-1). \end{aligned} \tag{8.30}$$

Hence the method is valid only if the exciting radiation is strictly unpolarized, i.e. $F = 1$.

Method 5

Here the *excitation* polarizer is set at $\phi = \cos^{-1}(2/3)^{1/2}$, and *no* emission polarizer is used, and again $\alpha = 90°$. This is the method recommended by Spencer and Weber (1970), but since in this case

$$\begin{aligned} R^\phi(90) &= T_V 2/3I_V^V(90) + 1/3I_V^H(90) + T_H 2/3I_H^V(90) + 1/3I_H^H(90) \\ &= 1/9kS^H T_H \tau(2FG + 2F - G - 1) + r(4FG - 2F - G - 1). \end{aligned} \tag{8.31}$$

the result will only be unbiased if $F = 1$, *and* $G = 1$.

Method 6

Here the excitation polarizer is set at $\phi = \cos^{-1}(1/3)^{1/2}$, the emission polarizer is vertical, and again $\alpha = 90°$. In this case, the response is

$$\begin{aligned} R_V^\phi(90) &= T_V[1/3I_V^V(90) + 2/3I_V^H(90)] \\ &= 1/9kS^H T_V \tau(F+2) + 2r(F-1) \end{aligned} \tag{8.32}$$

Again, the result is unbiased only if the excitation radiation is unpolarized, $F = 1$. *Use of any of the Methods 4, 5 and 6 therefore demands that scramblers be used to depolarize the exciting light and, in Method 5, the emitted light.* The emission scrambler should be placed between emission polarizers and dispersive element, if any, or between emission polarizer and detector. It would be as well at this juncture to note one further practical point concerning the use of polarizers. Glan prism polarizers are two half-prisms separated by a thin layer of air. The beam emerging from such a device is displaced with respect to the incident beam, and rotation of the polarizer causes the transmitted beam to deviate round a circle (Azumi and McGlynn, 1962). When used with an emission monochromator this causes *spectral* shifts of as much as 2 nm between vertical and horizontally polarized components

which can be critical when line spectra are being observed. Such effects are not found with flat plate polarizers, which although deficient in other respects, are much easier to use.

8.3 Time-dependent Anisotropy Measurements

The time dependence of anisotropy is obtained experimentally by measurement of the time dependence of the components of fluorescence polarized parallel $I_{||}(t)$, and perpendicular $I_{\perp}(t)$ to, say, vertically polarized excitation radiation, and is evaluated using Equations 8.3, 8.4 or 8.6.

Considerable care must be taken in making such apparently simple measurements. Some of the difficulties will now be discussed briefly.

8.3.1 Instrumental instability

Construction of $r(t)$ through Equation 8.6 involves the *difference* between $I_{||}$ and $I_{\perp}$ and this poses the first problem. To produce good statistics, it is essential that the difference be maximized; therefore the $I_{||}$ and $I_{\perp}$ curves must be collected to very high counts. Apart from the time consumed in this data collection, it increases the problems, discussed in earlier chapters, associated with excitation source instabilities, detection system drift, etc. These problems are not insurmountable, but require very careful attention to detail during the experiments; in particular, pulse profiles must be very strictly monitored before and after data collection to eliminate drift. Effects of changes in pump pulse profile can be minimized by simultaneous collection of $I_{||}$ and $I_{\perp}$.

A dual detection system can be utilized for this purpose, which, however, necessitates expensive duplication of equipment. Such a system is described by Tschanz and Binkert (1976) and is shown in Fig. 8.6. P_2 is the emission analysing polarizer which is kept fixed with the transmission direction perpendicular to the plane of the figure. For measurements of anisotropy, P_1 is rotated between the horizontal and vertical positions to measure $I_{\perp}(t)$ and $I_{||}(t)$, while the analyser P_3, in the reference channel, is positioned so that the direction of the transmitted component bisects the two positions of P_1, so that light detected through P_3 is independent of these positions of P_1. The alternation of *excitation* polarizer to obtain $I_{||}$ and $I_{\perp}$ rather than keeping P_1 fixed and altering P_2 has some advantages, particularly if a dispersive element is used to select some fluorescence wavelengths. The detection system polarizer, P_2, since it is not altered between measurements of $I_{||}$ and $I_{\perp}$, has the same response in each case, since light in the same polarization sense is always detected.

As an alternative to a polaroid sheet polarizer for P_1 with laser excitation, a half-wave plate may be used to change the plane of excitation radiation, though this has a disadvantage in that the spectral bandwidth of a half-wave plate is narrow. Half-wave plates are expensive and several will be required to span a given spectral range.

The method of determining time-dependent anisotropy with the system illustrated in Fig. 8.6 would be as follows. The excitation function, with a diffuse reflector in place of the sample, is measured. Then, with polarizer and

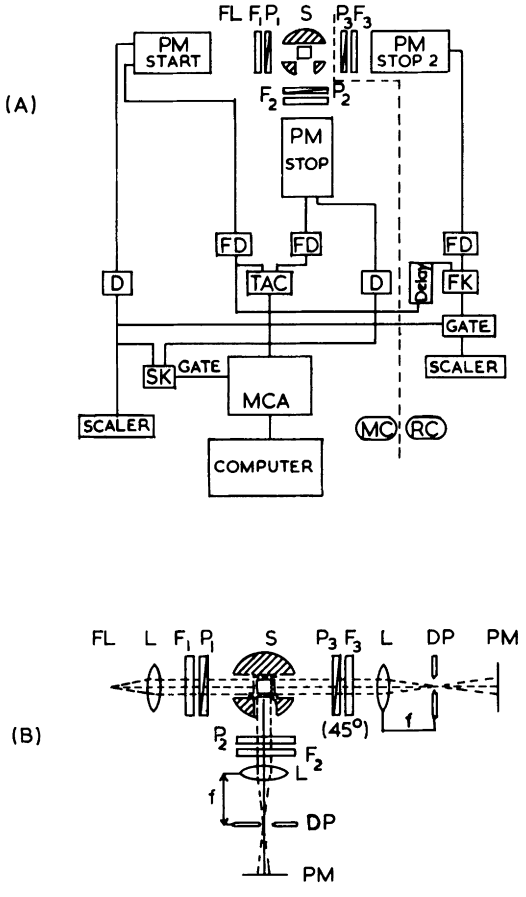

Figure 8.6 Dual detection single photon counting instrument. (A) Experimental arrangement. FL, flash lamp; S, sample; F_1, F_2, F_3, filters; P_1, P_2, P_3, polarizers; D, discriminator; FD, fast discriminator; MC, measuring channel; RC, reference channel; SK, slow coincidence; FK, fast coincidence. (B) Optical arrangement. Symbols as in (A) and L, lenses; DP, diaphragm (placed in the focal plane of the corresponding lens) (after Tschanz and Binkert, 1976).

analyser P_1 and P_2 parallel vertically, $I_{||}(t)$ is measured to a total of $m_{||}$ counts in the reference channel, 3. The polarizer P_1 is turned into the horizontal position, and a second measurement gives $I_{\perp}(t)$ and $m_{\perp}$. Before calculation of anisotropy, the intensity $I_{\perp}(t)$ must be normalized for identical excitation intensities, to $I_{||}(t)$ using the factor $m_{||}/m_{\perp}$.

As an alternative to the use of a reference channel, an experimental system can be set up in which there is a rapid alternation of observation of $I_{||}$ and $I_{\perp}$, for example, by using a two-position stepper-motor to rotate the detection polarizer between parallel and perpendicular positions on a time scale (e.g., 10 s) short compared with total data collection time. This ensures that the $I_{||}$ and $I_{\perp}$ curves are collected under identical conditions. A further non-trivial problem associated with the fact that difference curves are required involves the chemical and biological stability of samples under investigation during the long counting times.

8.3.2 Elimination of *G* factor

Even when fluorescence is not spectrally dispersed, care has to be taken to ensure that the *G* factor discussed above is unity, or if not, is taken into account in anisotropy measurements. There are several methods available to check this.

8.3.2(a) Tail-matching

Provided that $\tau_r < \tau_F$, it can be seen from Equations 8.3 and 8.4 that at long times after excitation, the curves for $I_{||}(t)$ and $I_{\perp}(t)$ as measured should become identical. If in any experiment they are not, it can usually be assumed that this is due to a non-unitary *G* factor. Hence normalizing the two decay curves on the tail of the decay eliminates the *G* factor. In Fig. 8.7 are shown uncorrected $I_{||}(t)$ and $I_{\perp}(t)$ curves for a macromolecular sample measured with laser excitation and a monochromator for dispersion of fluorescence. There is an obvious discrepancy. However, there are some serious drawbacks to tail-matching. First, the matching, or curve fitting, has to be done in a region of the decay where the statistics are poorest, with consequent errors. Secondly, counting to long times involves the use of a long timescale voltage ramp in the TAC, with consequent loss of precision at earlier times where anisotropy changes are most evident. The most serious drawback however is that there *are* systems for which the anisotropy is not expected to decay to zero during the fluorescence lifetime of the probe, e.g., in ordered or semi-ordered media such as liquid crystals, polymers of synthetic and biological origin, lipid bilayers, micelles, etc. Since these are the types of system most amenable to study by these techniques, the *assumption* implicit in tail-

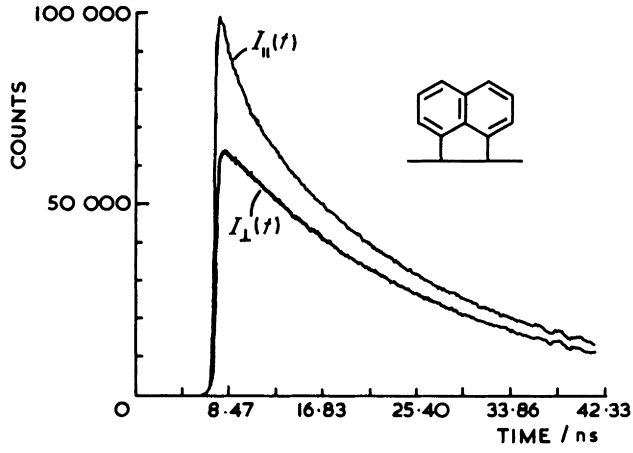

Figure 8.7 Decay of emission of acenaphthylene labelled polymethylmethacrylate in tetrahydrofuran. Laser excitation at 308 nm (after Drake *et al.*, 1982).

matching that r tends to zero is a dangerous one, unless checked carefully by other methods.

8.3.2(b) Leading edge matching

The initial anisotropy in a probe for which the emission and absorption transition dipoles have identical orientations with respect to the molecular framework is given by putting $\theta = 0$ in Equation 8.13, with the result that $r_0 = 2/5$. In any experimental system r_0 may be measured to be other than 2/5, and one of the causes of this is the G factor. If all other causes of deviations from the 2/5 result can with certainty be eliminated, then the G factor correction can be applied by weighting the $I_{\parallel}(t)$ and $I_{\perp}(t)$ decay curves such that the constructed anisotropy curve has $r_0 = 2/5$. This is an even more hazardous procedure than tail-matching, since it is not usually possible to be certain what the initial anisotropy should be. There are many probes for which the spectroscopy is complex, leading to a much reduced r_0. In addition, as the data in Table 8.1 illustrate, r_0 values can be different from 0.4 depending on the nature of the photoselection and the viewing geometry.

Moreover, leading edge matching requires manipulation of decay curves in the region where convolution with instrument response and excitation functions (see below) are of greatest importance.

Table 8.1 Polarization ratios and r_0 values in idealized photoelectron experiments (developed from Albrecht, 1970).

	Exciting light unpolarized				Exciting light vertically polarized			
	Head on viewing		90° viewing		Head on viewing		90° viewing	
Photoselection/observe	$(I_{\|\|}/I_\perp)$	r_0	$(I_{\|\|}/I_\perp)_0$	r_0	$(I_{\|\|}/I_\perp)_0$	r_0	$(I_{\|\|}/I_\perp)_0$	r_0
Single axis/same axis	1	0	2/1	0.2	3/1	0.4	3/1	0.4
Single axis/perp. axis	1	0	3/4	−0.1	1/2	−0.2	1/2	−0.2
In-plane/out-of-plane	1	0	3/4	−0.1	1/2	−0.2	1/2	−0.2
In-plane/out-of-plane	1	0	7/6	0.05	4/3	0.1	4/3	0.1

8.3.2(c) Use of a freely-rotating probe

Perhaps the simplest method of evaluating G factors is to use a probe fluorophore, the rotational relaxation time of which is very short compared with the decay time, and to carry out a continuous illumination experiment in the manner described in Section 8.2. Such a procedure carried out on our own experimental system using α-cyanonaphthalene in cyclohexane as calibrant, $\tau_F = 18.8$ ns, yielded a G factor of 1.03. Use of this to correct the $I_{||}(t)$ and $I_{\perp}(t)$ curves shown in Fig. 8.7 showed quite clearly that there was *no* residual anisotropy in this sample, and hence that tail-matching would have been justified. The result of tail-matching, shown in Fig. 8.8, is identical to that resulting from application of the G factor correction, although extreme care is needed to ensure that this is so.

8.3.2(d) Synthesis of fluorescence decay curve

The total fluorescence decay of a fluorophore is given by Equation 8.5 as being $I_{||}(t)+2I_{\perp}(t)$ for plane polarized excitation. If $I_{||}(t)$ and $I_{\perp}(t)$ are measured separately, they can be combined with a suitable weighting factor, such that the synthesized fluorescence decay curve $I_{||}(t)+2GI_{\perp}(t)$ matches exactly that measured under experimental conditions that eliminate effects of polarisation (e.g., Method 2, Section 8.2). This procedure evaluates non-unit

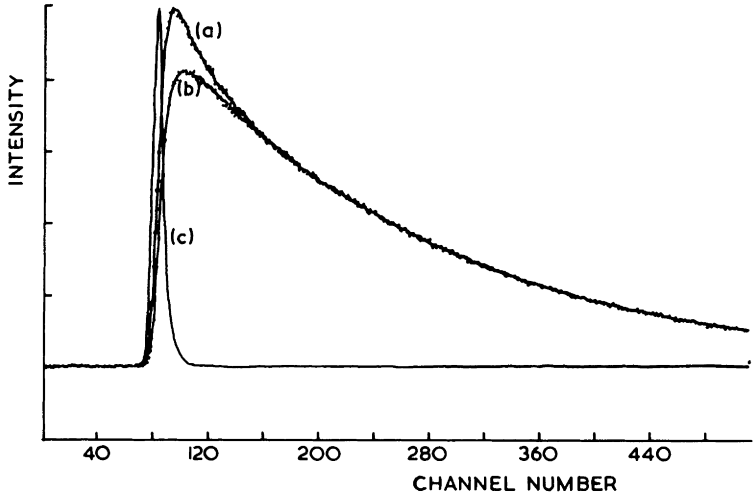

Figure 8.8 Illustration of tail-matching applied to $I_{||}$(a) and $I_{\perp}$(b) curves for the sample described in Fig. 8.7. Points are the observed data and the lines are best fit curves. (c) Instrument response function. 0.082 ns per channel.

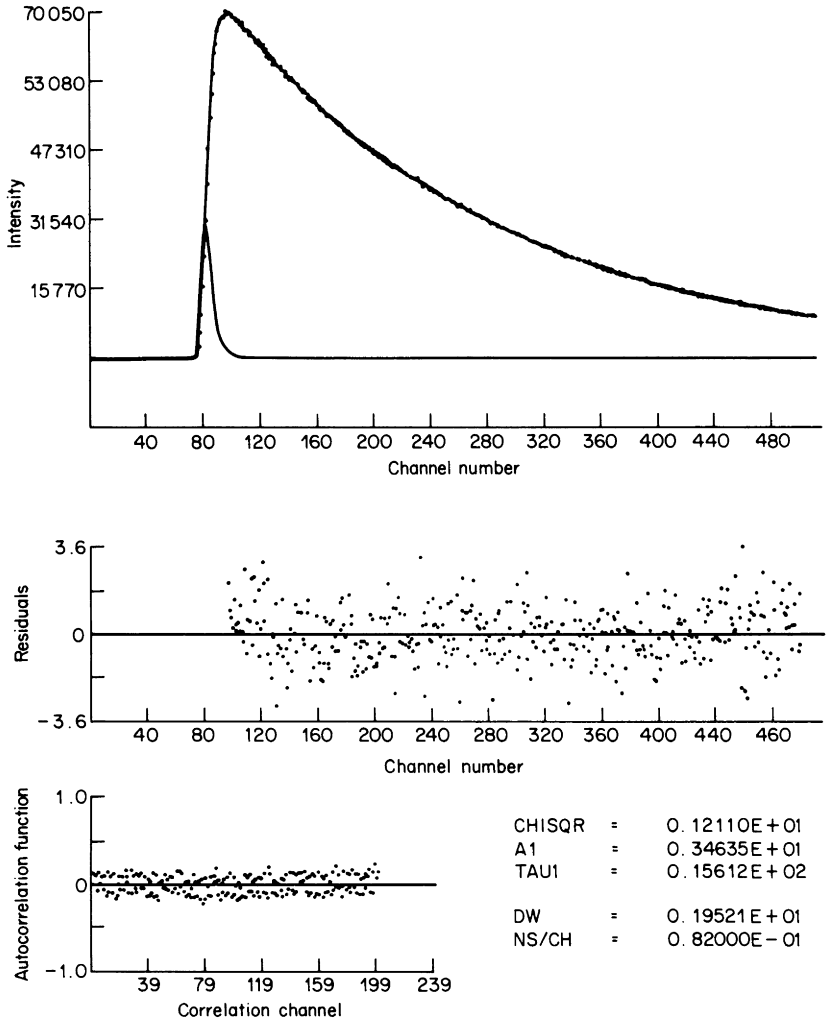

Figure 8.9 Synthesis and analysis of $I_{||} + 2.06I_{\perp}$ for the sample described in Fig. 8.7. Upper section: data synthesized from observed $I_{\perp}$ and $I_{||}$ (points), best fit curve (line) and instrument response function (small peak to the left). Middle section: plot of weighted residuals. Lower section: autocorrelation function of weighted residuals. Weighting factors given by Equation 8.36.

G factors in the system. Its application to a macromolecular sample is illustrated in Fig. 8.9.

A variation on this method is to use either Equation 8.3 or 8.4 to fit the $I_{||}(t)$ curve or $I_{\perp}(t)$ curve, weighting such that the value of τ_F recovered

matches that from "magic angle" excitation, although this procedure requires some assumption of the functional form (single component, multiple exponential) for τ_r. In our experience this method is quite successful; for when the double exponential fitting routine (e.g., that listed in Appendix 6.A2) is used to analyse $I_{\parallel}(t)$ and $I_{\perp}(t)$ according to Equations 8.3 and 8.4 identical results are obtained, as indicated in Fig. 8.10. However, there may be

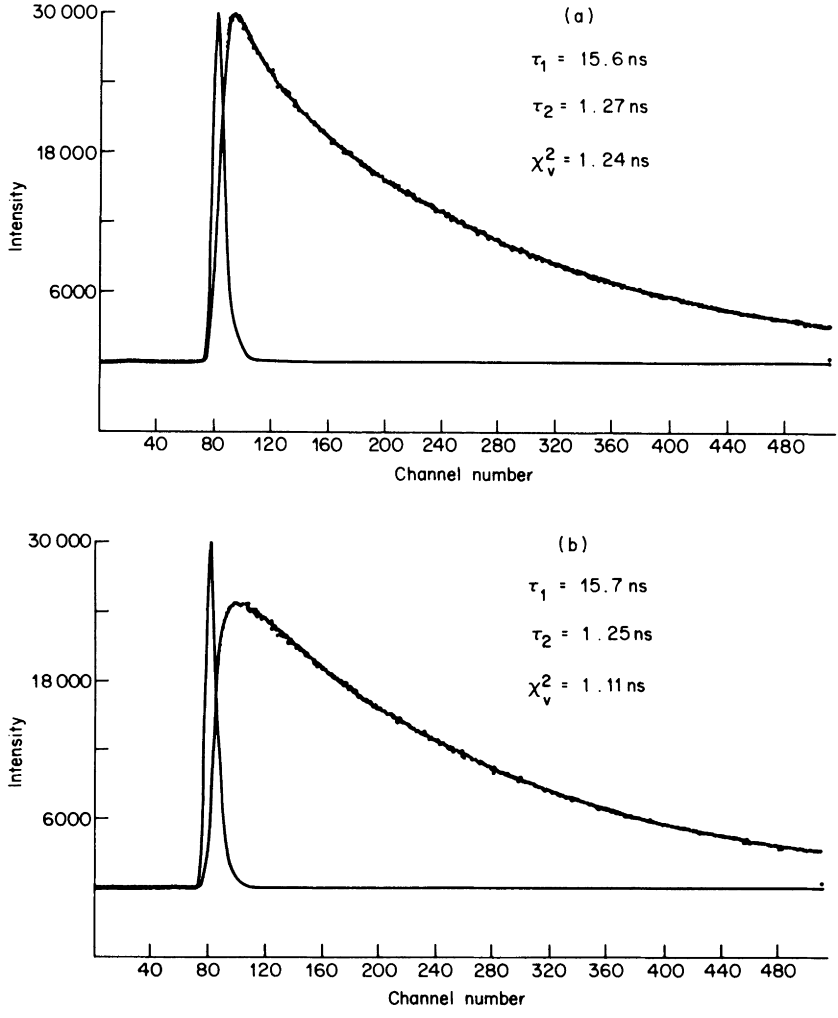

Figure 8.10 Separate analyses of $I_{\parallel}(t)$ and $I_{\perp}(t)$ for the sample described in Fig. 8.7, 0.082 ns per channel. The curves (lines and points) have the usual signification. (a) $I_{\parallel}(t)$ analysed according to Equation 8.3. (b) $I_{\perp}(t)$ analysed according to Equation 8.4.

uncertainties about the single value of τ_r resulting from this procedure, especially if the intrinsic fluorescence decay is non-exponential.

It is strongly recommended that combinations of all of the above methods are used vigilantly to ensure the reproducibility of data in these experiments.

8.4 Deconvolution Procedures

As we have stated above, much of the information concerning change in anisotropy with time will be contained in the early portions of fluorescence decay curves, where the effects of finite excitation profile and instrument response functions will be greatest. In such cases, some form of deconvolution will be essential in order to obtain reliable data, but the best procedure to adopt is still the subject of strenuous debate. It would of course be preferable if deconvolution were unnecessary, but this can only be realized in a small number of cases, using narrow temporal bandwidth excitation and very fast detection. Using the least-squares fitting routine favoured by us, the possibilities are outlined in Sections 8.4.1–8.4.4 with respect to a single polymer sample, and results are compared.

8.4.1 Create anisotropy r, from $I_{||}(t)$, $I_{\perp}(t)$ without deconvolution

This procedure yields two components of τ_r, but with considerable question concerning the shorter of the two.

8.4.2 Analyse $I_{||}(t)$ or $I_{\perp}(t)$ to obtain τ_F, τ_r from Equations 8.3 and 8.4

This was shown in Fig. 8.10. The CREWS program recovered τ_F accurately, but was able to recover, of course, only one τ_r value. Attempts to use a triple exponential fitting program to investigate other rotational components were unsuccessful. Clearly this method deconvolves out instrument response and finite excitation effects, and since complete decays are used the quality of data is such that confidence in values of τ_F and τ_r recovered should be high. However, for dual component anisotropies, successful recovery of the information requires a triple component fit to the data, since τ_F also appears as a term in the relevant equations, and even with excellent quality data, the occasions upon which six parameter fits can be applied with confidence are few.

8.4.3 Create difference, $[I_{||}(t) - I_{\perp}(t)]$, then deconvolve

It can be seen from Equations 8.3 and 8.4 that

$$I_{||}(t) - I_{\perp}(t) = 3r_0 e^{-t/\tau_r} e^{-t/\tau_F}. \tag{8.33}$$

Deconvolved curves can be fit to this function, and if τ_F is known from a separate experiment (e.g. magic angle viewing), τ_r can be recovered. For multiple components of τ_r, however, there are the same difficulties as in Method 8.4.2, but aggravated by the fact that *difference* curves have much poorer signal-to-noise ratios, and curve fitting procedures are even more subject to error. An example of deconvolving a difference curve of this type is illustrated in Fig. 8.11.

8.4.4 Deconvolve $I_{||}(t)$, $I_{\perp}(t)$ using arbitrary function, create $r(t)$

This is the method we favour in principle. If $I_{||}(t)$ and $I_{\perp}(t)$ are deconvolved, separately, in terms of *arbitrary* fitting functions, for example using the ten exponential program given in Appendix 7.A1, no functional form has to be assumed for either of these curves. Construction of the anisotropy from the resulting functions is straightforward and the time-dependent anisotropy curves, now free of convolution effects, can be analysed by curve fitting methods which in principle should yield data of greater reliability, since the expression for $r(t)$ does *not* contain terms in τ_F. The drawback is again that of relying upon a *difference* of two curves, with consequent loss of quality of data. This seems to be an unavoidable problem.

8.4.5 Weighting factors for anisotropy experiments

In fitting decays using the least-squares technique the fit is usually weighted according to Equation 8.34 (see also Equation 2.11):

$$w_i = \frac{1}{\sigma_i^2} = \frac{1}{I(t_i)}. \tag{8.34}$$

$I_{||}(t)$ and $I_{\perp}(t)$ obey Poisson statistics and can be deconvolved in the usual way using this equation for weighting. If we wish to deconvolve $I_{||}(t) - I_{\perp}(t) = d(t)$, $I_{||}(t) + 2I_{\perp}(t) = s(t)$ and $r(t) = d(t)/s(t)$ we must calculate the weighting factors by propagating the Poisson errors in the measured curves. It is easy to derive the following equations (Wahl, 1979):

$$\text{for } d(t_i), \qquad w_i = \frac{1}{I_{||}(t_i) + I_{\perp}(t_i)} \tag{8.35}$$

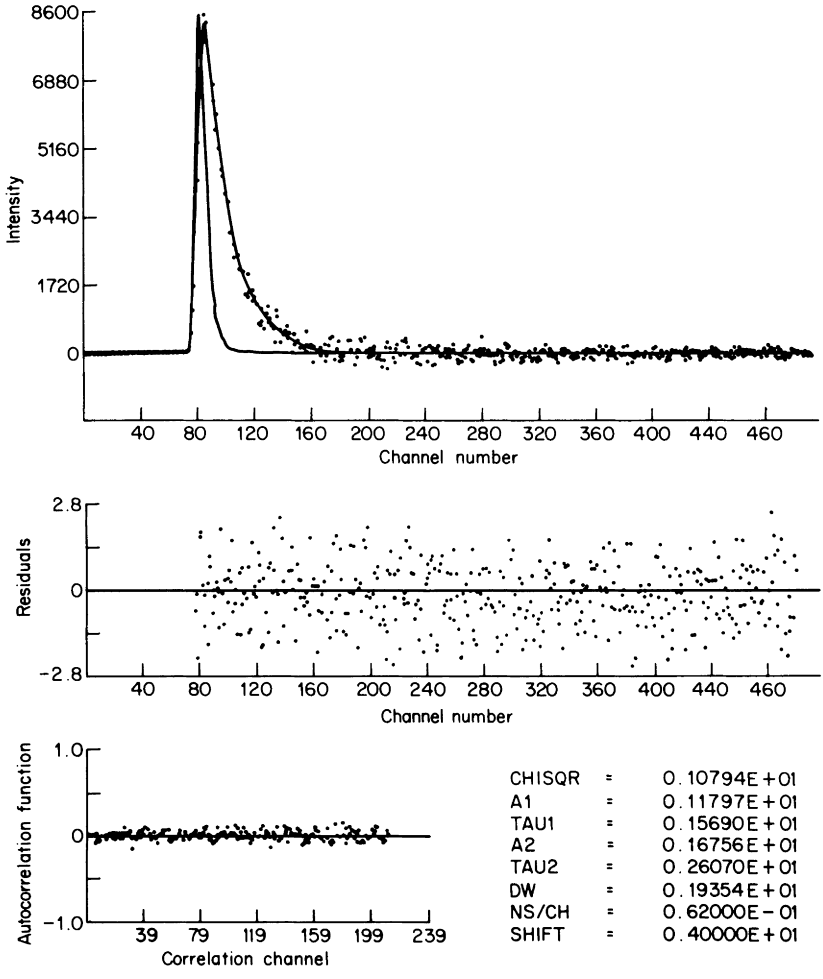

Figure 8.11 Analysis of the difference function $d(t) = I_{||}(t) - I_{\perp}(t)$ for the sample described in Fig. 8.7. Analysing function: Equation 8.33. Upper section: $d(t)$ calculated from observed data (points), best fit curve (line) and instrument response function (curve on l.h.s. of points). Middle section: weighted residuals. Lower section: autocorrelation function of weighted residuals. Correct weighting factors (Equation 8.35) were used.

$$\text{for } s(t_i), \qquad w_i = \frac{1}{I_{||}(t_i) + 4I_{\perp}(t_i)} \tag{8.36}$$

$$\text{and for } r(t_i), \qquad w_i = \frac{3[I_{||}(t_i) + 2I_{\perp}(t_i)]}{2 + r(t_i) + 5[r(t_i)]^2 - 2[r(t_i)]^3}. \tag{8.37}$$

Clearly $d(t_i)$, $s(t_i)$ and $r(t_i)$ are not Poisson distributed and use of incorrect weighting factors may lead to grossly incorrect results, as illustrated in Fig. 8.12 where analysis of the difference function $d(t)$ with (incorrect) weighting factors given by $w_i = 1/[I_{\parallel}(t_i) - I_{\perp}(t_i)]$ is shown. Analysis of this function with correct weighting factors is shown in Fig. 8.11 and it will be seen that the results are quite different. In particular the incorrect value for τ_r is almost an order of magnitude too small.

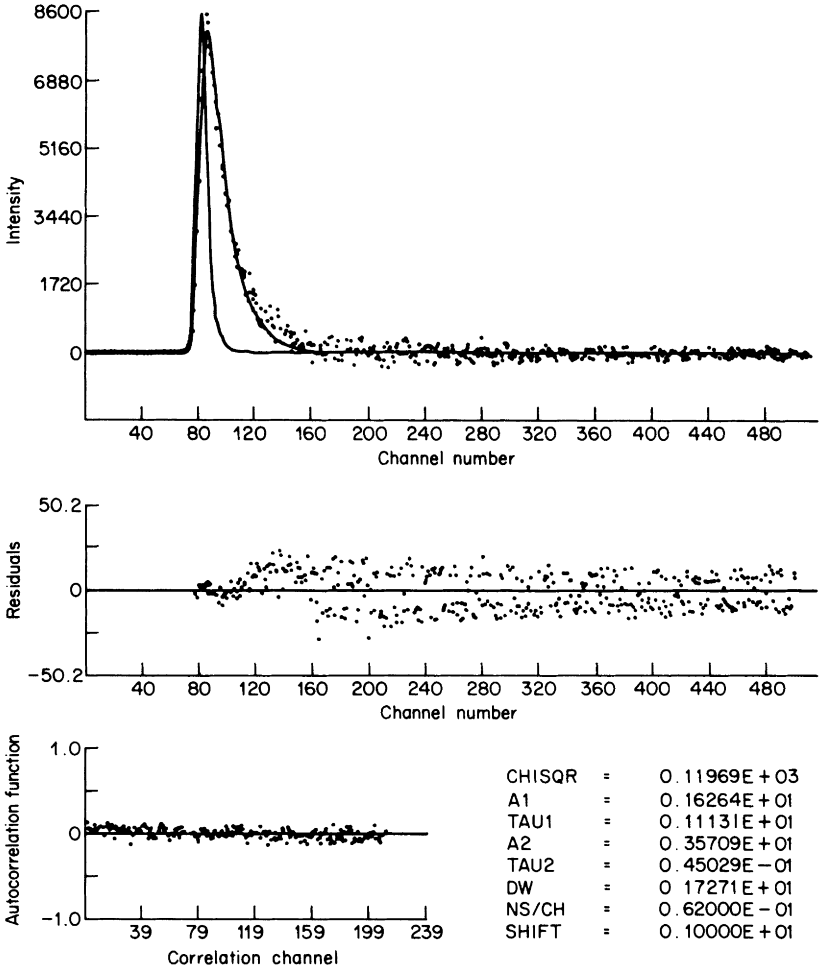

Figure 8.12 The difference function $d(t)$, described in Fig. 8.11 analysed using incorrect weighting factors (see text). Note the poor χ^2_v value and the large discrepancy in τ values between this and the correct analysis (Fig. 8.11).

8.4.6 Fitting by means of Lagrange multipliers

Methods other than least-squares fitting routines have been attempted to recover $r(t)$. For example the use of a Lagrange multiplier technique (Andre *et al.*, 1982) is illustrated in Fig. 8.13, in which fluorescence from an anthra-

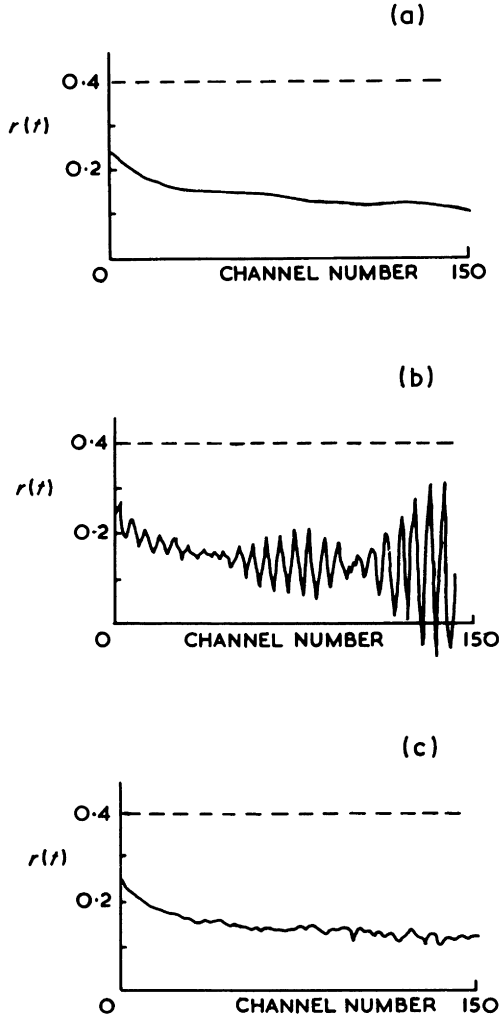

Figure 8.13 The decay of anisotropy of an anthracene probe inserted in a polybutadiene chain. Deconvolution of $[I_{\|}(t)-I_{\perp}(t)]/[I_{\|}(t)+2I_{\perp}(t)]$ using (a) exponential series, (b) Fourier transforms and (c) regularized Lagrange multipliers (after Andre *et al.*, 1982).

Table 8.2 Comparison of three "non *a-priori*" methods in analysing the total decay $[I_{||}(t)+2I_{\perp}(t)]$ of the probe anthracene in a polybutadiene chain (after Andre *et al.*, 1982).

Method	χ^2/χ^2 Lagrange
Exponential series	5.2
Fourier transform	2.3
Lagrange	1

cene fluorophore in the centre of a poly(butadiene) chain is analysed by least-squares fitting (Section 6.5.8), fast Fourier transform (Section 6.5.6), and Lagrange multiplier (Section 6.5.8) methods. Table 8.2 shows that the χ^2 values from this technique are superior to those from the other methods. Although this is still a good indicator of the relative quality of fitting, absolute values of χ^2 have no meaning in these cases, since *differences* of two curves are used in the construction of $r(t)$.

The discussions above will have served to illustrate that reliable values of $r(t)$ are difficult to obtain experimentally. It is pertinent to explore, however, how $r(t)$ should in principle be related to the motion of molecules. This is now discussed.

8.5 Theory of Time-dependent Fluorescence Depolarization

Following Tao (1969), the problem can be stated as follows. In Fig. 8.14, x, y, and z are the space-fixed coordinate system in the laboratory, with the sample placed at the origin. The exciting light travels along the x-axis, polarized with the electric vector e along the z-axis. The fluorescence, polarized along the z-axis, $(I_{||})$ and the x-axis, $(I_{\perp})$ will be observed along the y-axis. $\bar{\mu}$ is the transition dipole of the molecule, and θ, ϕ here, in contrast to the use of θ earlier in this chapter, define the orientation of $\bar{\mu}$ with respect to the space-fixed axes. What is sought is an expression for $r(t)$. The derivations will not be given here, but the reader is referred to a recent article by Lipari and Szabo (1980) and to earlier work by Belford *et al.* (1972), Tao (1969), Lombardi and Dafforn (1966), and Weber (1971). There was originally some dispute about the solution for $r(t)$, but the correct form for the emission anisotropy for a general rotating body was derived by Belford *et al.* (1972) and was found to contain five exponential terms:

$$\frac{5}{6}r(t)=\sum_{i=1}^{3} C_i \exp(-t/\tau_i)+[(F+G)/4]\exp(-6D-2\Delta)t + [(F-G)/4]\exp[-(6D+2\Delta)t] \tag{8.38}$$

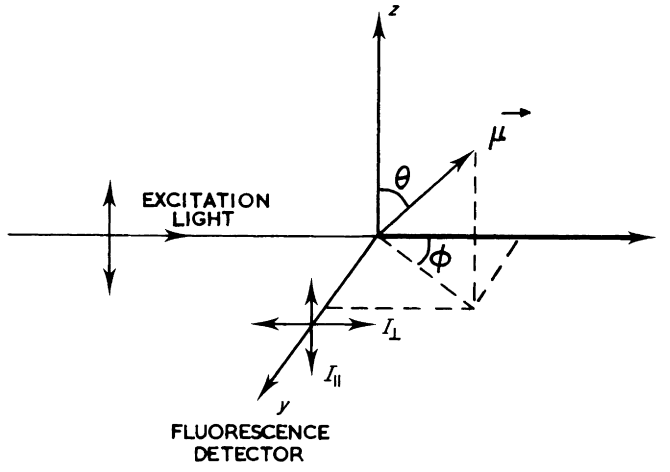

Figure 8.14 Experimental geometry for time-resolved fluorescence depolarization measurements.

where $D=(D_1+D_2+D_3)/3$, the mean rotational diffusion constant, given that D_1, D_2 and D_3 are the rotational diffusion constants around the three principal axes of the molecule labelled 1, 2 and 3 (to be distinguished from the laboratory axes labelled x, y and z in Fig. 8.14).

$$\Delta=(D_1^2+D_2^2+D_3^2-D_1D_2-D_1D_3-D_2D_3)^{1/2}.$$

$$C_i=\alpha_j\alpha_k\varepsilon_j\varepsilon_k \qquad \text{where } (ijk)=(1\,2\,3),(2\,3\,1) \text{ or } (3\,1\,2).$$

$\alpha_1, \alpha_2, \alpha_3$ are the direction cosines of the absorption dipole with respect to the

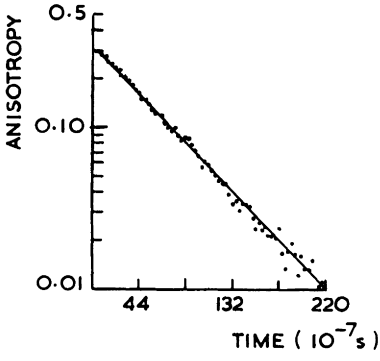

Figure 8.15 Decay of emission anisotropy simulated by computer (points) and compared with the prediction based on Equation 8.38 (line) (after Harvey and Cheung, 1972).

principal rotation axes. ε_1, ε_2 and ε_3 are, likewise, the direction cosines of the emission dipole.

$$\tau_i = (3D + 3D_i)^{-1}$$

$$F = \sum_{i=1}^{3} \alpha_i^2 \varepsilon_i^2 - 1/3$$

$$G\Delta = \sum_{i=1}^{3} D_i(\alpha_i^2 \varepsilon_i^2 + \alpha_j^2 \varepsilon_k^2 + \alpha_k^2 \varepsilon_j^2) - D \qquad (i \neq j \neq k \neq i)$$

It can be seen that Equation 8.38 represents $r(t)$ in terms of five exponential terms, which is rigorously correct. However, although each of these terms contributes to the time dependence of fluorescence, no more than three are independent and in most realistic experimental circumstances only two, or in extremely favourable cases, three (Small and Isenberg, 1977), decay rates will be distinguishable. Furthermore, as Belford *et al.* (1972) point out, any one of these experimental rates will usually be proportional to some weighted average of the five intrinsic decay rates represented by Equation 8.38. It should be stated that treatments by Lombardi and Dafforn (1966) and Weber (1971), which both predicted *two* decay times only, are not the consequence of any error, but reflect special symmetry restrictions in one case, discussed below, and the adoption of a six-position jump model in the other. In general α and ε values are not available, in which case weighting factors are not well known, and it has been suggested that the two decay times in Weber's model, being functions of α and ε, can properly be regarded as the two phenomenological decay rates which will ensue from any experiment. It should be further noted that the treatment by Tao (1969), which again predicts five exponential decay terms, is a special case, being valid only when the absorption and emission dipoles have coincidental directions ($\alpha_i = \varepsilon_i$ for all i), and also errs in that a simple one-to-one correspondence between the distribution of body orientations and the distribution of orientations of emitting dipoles is assumed. Computer simulated data have been used to check the validity of the general expression (Harvey and Cheung, 1972). In all cases good agreement was observed between the simulated data and theoretical curves. The results for one such experiment are shown in Fig. 8.15. It is possible in some cases to observe an initial increase in $r(t)$ as a consequence of the orientation of the absorption and emission dipoles.

There are several special cases resulting from the general expression. For a body that possesses an axis of symmetry, such as an ellipsoid of rotation, we may define

$$D_1 = D_2 = D_\perp$$

$$D_3 = D_{||}$$

The emission anisotropy in this case is given by (Tao, 1969):

$$r(t) = \frac{2}{5}\{A_1(\delta)\exp(-6D_\perp t) + A_2(\delta)\exp[-(5D_\perp + D_{||})t]\}$$
$$+ A_3(\delta)\exp(2D_\perp + 4D_{||}), \tag{8.39}$$

where

$$A_1(\delta) = (3/2\cos^2\delta - \tfrac{1}{2})^2,$$
$$A_2(\delta) = 3\cos^2\delta\sin^2\delta,$$
$$A_3(\delta) = \tfrac{3}{4}\sin^4\delta,$$

and δ is the angle between the emission (and absorption) transition dipole and the axis of symmetry. For the special case in which δ is 90° (e.g. the dipole is oriented perpendicular to the axis of symmetry):

$$r(t) = \frac{1}{10}[\exp(-6D_\perp t) + 3\exp[-(2D_\perp + 4D_{||})t]] \tag{8.40}$$

and for the dipole parallel to the axis ($\delta = 0$) the equation for $r(t)$ is reduced to a single exponential term:

$$r(t) = \frac{2}{5}\exp(-6D_\perp t). \tag{8.41}$$

For a rotating spherical body, the correlation function of order n is given by (Williams, 1978):

$$\langle P_n[\hat{\mu}(0)\cdot\hat{\mu}(t)\rangle = \exp[-n(n+1)D_r t)]. \tag{8.42}$$

Hence, for fluorescence depolarization measurements in which the second order correlation function is desired

$$r(t) = \frac{2}{5}\exp(-6D_r t). \tag{8.43}$$

Here D_r is the rotational diffusion constant and is given by the Einstein law as

$$6D_r = \frac{1}{\tau_r} = \frac{kT}{V\eta}, \tag{8.44}$$

where V is the volume of the sphere and η is the viscosity of the solvent. Some confusion exists in the definition of the rotational relaxation time τ_r; many reports preferring $\rho_0 (= 3\tau_r)$.

The three decay constants appearing in the expression for $r(t)$ for an ellipsoid of rotation have been calculated and are shown in Table 8.3. As may be seen, the three relaxation times diverge rapidly with increasing axial ratio

Table 8.3 Rotational diffusion decay constants for prolate and oblate ellipsoids

ρ	$1/\rho$	$\tau_{\|\|}/\tau_r$	τ_1/τ_r	τ_2/τ_r	τ_3/τ_r
Prolate ellipsoids					
1		1.0000	1.0000	1.0000	1.0000
2		0.8067	1.5049	1.3152	0.9543
3		0.7480	2.3408	1.7276	0.9674
4		0.7210	3.3956	2.0984	0.9777
5		0.7061	4.6405	2.4060	0.9842
6		0.6968	6.0616	2.6548	0.9884
7		0.6906	7.6506	2.8549	0.9911
8		0.6862	9.4008	3.0162	0.9930
9		0.6829	11.3080	3.1472	0.9944
10		0.6805	13.3680	3.2545	0.9954
15		0.6739	25.8607	3.5774	0.9979
20		0.6712	41.8199	3.7280	0.9988
Oblate ellipsoids					
1		1.0000	1.0000	1.0000	1.0000
2		1.4100	1.1316	1.1701	1.3032
3		1.8284	1.4645	1.5147	1.6885
4		2.2495	1.8431	1.9003	2.0955
5		2.6718	2.2398	2.3018	2.5104
6		3.0948	2.6455	2.7111	2.9290
7		3.5181	3.0564	3.1247	3.3495
8		3.9418	3.4705	3.5411	3.7711
9		4.3655	3.8869	3.9593	4.1934
10		4.7894	4.3049	4.3787	4.6162
15		6.9099	6.4073	6.4859	6.7338
20		9.0312	8.5193	8.6005	8.8538

ρ is the axial ratio (ratio of longitudinal semi-axis to equatorial semi-axis), $\tau_{\|\|}=(6D_{\|\|})^{-1}$, $\tau_1=(6D_\perp)^{-1}$, $\tau_2=(5D_\perp+D_{\|\|})^{-1}$, $\tau_3=(2D_\perp+4D_{\|\|})^{-1}$, $\tau_r=(6D_r)^{-1}$ is the relaxation time under the spherical model. Adapted from Tao (1969).

for a prolate ellipsoid. However, for an oblate ellipsoid the deviations are small even for high axial ratios and experimentally it may prove difficult to resolve more than a single, mean relaxation time for $r(t)$ in this case. Thus, three situations exist in which the emission anisotropy may decay exponentially and it is not possible, therefore, to distinguish: (1) a true spherical geometry; (2) oblate geometry; (3) preferential orientation of the fluorescence probe with respect to the principal axis. Hence, it should be stressed, a single exponentially decaying emission anisotropy does *not* correspond uniquely to a spherical rotating body. On the other hand, the observation of non-exponential behaviour of $r(t)$ indicates deviations from spherical behaviour if the probe is known to have parallel absorption and emission dipoles. If the

latter condition is not true, a spherical rotating molecule will also give rise to multiple component anisotropies.

8.6 Form of Time-dependent Anisotropy for Restricted Motion

The form for the emission anisotropy in several special cases is of interest. The decay of the anisotropy for a chromophore rotating between two barriers has been derived by Wahl (1975). The problem posed by a fluorophore with restricted rotation in an ordered lipid bilayer has been discussed by Kinoshita *et al.* (1977). If r_0 is the initial anisotropy created in the system at time 0 and r_∞ is the final limiting value after long times, than, as opposed to an isotropic, low viscosity solvent, r_∞/r_0 will not be zero, but will be a measure of the degree of confinement of the orientation of the label imposed by the architecture of the membrane. The decay in $r(t)$ between these two limits should reflect the degree of "wobbling" motions possible for the fluorophore. The case is illustrated in Fig. 8.16, where θ here is the orientation angle of a cylindrical probe with respect to the axis of a bilayer. Kinoshita *et al.*'s analysis leads to:

$$\frac{r(t)}{r(0)} = \langle P_2[\hat{\mu}(0)\cdot\hat{\mu}(t)\rangle = \sum_i A_i \exp^{(-D_w t/\sigma_i)}, \tag{8.45}$$

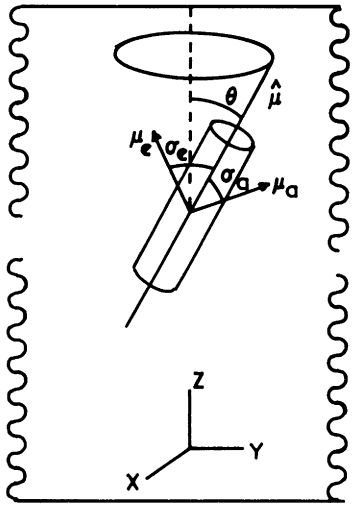

Figure 8.16 Schematic outline of a cylindrical fluorescent probe embedded in a lipid bilayer. θ is the (variable) orientation angle of the probe with respect to the axis of the bilayer and θ_0 (not shown) is the maximum value of θ (after Lipari and Szabo, 1980).

where D_w is the "wobbling" diffusion constant, which will be of magnitude greater than that for an unrestricted motion. The coefficients A_i and σ_i cannot be expressed as closed analytical functions of θ, defined in Fig. 8.16, but Kinoshita *et al.* have displayed these graphically, and in addition, have presented an approximate expression for $r(t)/r(0)$, Equation 8.46:

$$\left[\frac{r(t)}{r(0)}\right]_{\text{approx.}} = A_\infty + (1 - A_\infty)\exp(-D_w t/\langle\sigma\rangle), \tag{8.46}$$

where $A_\infty = r(\infty)/r(t)$ and is given by

$$\frac{r(\infty)}{r(0)} = \langle P_2(\cos\theta)\rangle^2$$

$$= [(\tfrac{1}{2}\cos\theta_0(1+\cos\theta_0)]^2. \tag{8.47}$$

θ_0 is the semi-angle of the cone in which the probe is free to wobble, and

$$\langle\sigma\rangle = \sum_{i\neq\infty} A_i\sigma_i/(1 - A_\infty). \tag{8.48}$$

This treatment is approximate, but Lipari and Szabo (1980) have shown that an exact solution is possible. The result is then

$$D_w\tau_{\text{eff}}(1 - A_\infty) = -x_0^2(1+x_0)^2\{\log[(1+x_0)/2]$$
$$+(1-x_0)/2\}/[2(1-x_0)]$$
$$+(1-x_0)(6+8x_0-x_0^2-12x_0^3-7x_0^4)/24 \tag{8.49}$$

where $x_0 = \cos\theta_0$. Hence measurement of A_∞ yields a value for the "wobble" angle θ_0, and even if $r(t)/r(0)$ is not adequately represented by a single exponential, Equation 8.49 allows extraction of D_w from the decay of the emission anisotropy, since $\tau_{\text{eff.}}(1 - A_\infty)$ is exactly the area under $[r(t) - r(\infty)/r(0)]$. These expressions are valid *only* if either the absorption, μ_a, or emission, μ_e, dipole lies along the C_∞ axis μ of the probe. However, Lipari and Szabo (1980) have given an approximate solution for the general case, which will be discussed presently. For the moment, again assuming μ_a or μ_e coincides with the μ axis, the case of the probe molecule attached to a macromolecule can be considered. In this case, the approximate Equation 8.46 becomes:

$$\frac{r(t)}{r(0)_{\text{approx.}}} = A_\infty\exp(-t/\tau_M)$$
$$+(1 - A_\infty)\exp[-t(\tau_M^{-1} + \tau_{\text{eff.}}^{-1})], \tag{8.50}$$

where $\tau_M = D_M/6$, D_M being the rotational diffusion coefficient of the macromolecule.

This is exactly the form of the expression used empirically by Munro *et al.* (1979) to analyse data on the anisotropy of tryptophan fluorescence of a variety of proteins, when $\tau_M \gg \tau_{eff.}$ (a good approximation in many cases). The expression used by these authors to relate their effective correlation time to D, however, did not have a sound theoretical basis, and a reasonably accurate approximation is

$$\tau_{eff.} = 7\theta_0^2/24D_w \tag{8.51}$$

even at large cone angles. However, it seems clear that tryptophan is a poor probe in that the conditions inherent in the use of Equation 8.50 that the absorption or emission dipole is parallel to the axis which wobbles, are certainly not satisfied.

For the case where neither μ_a or μ_e are coincident with the C_∞ axis, an approximate solution has been given (Lipari and Szabo, 1980). It is

$$\left[\frac{r(t)}{r(0)}\right]_{approx.} = \frac{e^{-t/\tau_M}}{P_2(\cos\delta)} \sum_{m=-2}^{2} e^{-m^2t/6\tau_e'}[S^2 + (1-S^2)e^{-t(1-m^2/6)/\tau_e'}] \times d_{m0}(\theta_e)d_{m0}(\theta_a)\cos m\phi_{ae}, \tag{8.52}$$

where θ_e and θ_a are the angles between μ_a and μ_e and μ respectively, δ is as before the angle between μ_a and μ_e, ϕ_{ae} is the difference between their azimuthal angles, τ_e'' is an effective correlation time for the wobbling of the $\hat{\mu}$ axis, and $d^2_{Mo}(\beta)$ are reduced Wigner rotation matrices, that is

$$d_\infty^{(2)}(\beta) = (3\cos^2\beta - 1)/2 \tag{8.53}$$

$$d \pm 10(\beta) = \frac{4}{4}(3/2)^{1/2}\sin\beta\cos\beta \tag{8.54}$$

$$d \pm 20(\beta) = (3/8)^{1/2}\sin\beta^2\beta \tag{8.55}$$

The sum over m in Equation 8.52 contains only three unique terms. As required, when θ_a or θ_e equals zero, Equation 8.52 reduces to Equation 8.50, with $\tau_e'' = \tau_{eff.}$, and when $\theta_0 = \pi$, i.e., the motion is unrestricted, and $\tau_M = \infty$, it reduces to the result for a freely diffusing cylinder with $\tau_e' = 1/6D_2$ and $\tau_e'' = 1/6Dx$.

There have been many other models of varying complexity which have been used to interpret time-dependent rotational anisotropy $r(t)$. We mention further here only the rather restricted model which attempts to mimic segmental motion of synthetic macromolecules (Valeur and Monnerie, 1976) by placing the chains upon a diamond lattice, and permitting only three and four centre motions upon this tetrahedral lattice, Fig. 8.17. The emission anisotropy in this case is given by

$$r(t) = r_0\exp(-t/\rho)\,\mathrm{erfc}\,(t/\rho)^{1/2}, \tag{8.56}$$

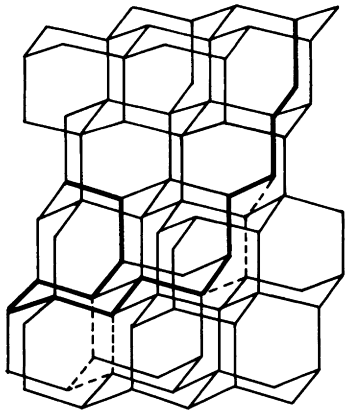

Figure 8.17 Schematic representation of a chain on a tetrahedral lattice (after Valeur and Monnerie, 1976).

where ρ is an effective relaxation time, and erfc is the error function complement. When valence angles and internal rotation angles are allowed to vary from an ideal lattice, and additional exponential term is introduced (Dubois-Violette *et al.*, 1969), and the expression for $r(t)$ becomes

$$r(t) = r_0 \exp(-t/\sigma) \exp(-t/\sigma) \operatorname{erfc}(t/\rho)^{1/2}, \tag{8.57}$$

where σ is a relaxation time reflecting the relaxation with respect to the ideal lattice.

Experimental measurements have in general yielded at most two, and often only one component decays in the analysis of $r(t)$. It is very clear from the discussions above that interpretation of $r(t)$ is far from straightforward, and that meaningful progress will only be made if experimental determinations of $r(t)$ can be made much more precisely than has in general been the case to date.

References

Albrecht, A. C. (1970). *Prog. React. Kinet.* **5**, 301–334.

Andre, J. C., Viovy, J. L., Bouchy, M., Vincent, L. M. and Valeur, B. (1982). In "Deconvolution and Reconvolution of Analytical Signals" (Bouchy, M., ed.), pp. 223–246. E.N.S.I.C.–I.N.P.L., Nancy.

Azumi, T. and McGlynn (1962). *J. Chem. Phys.* **37**, 2413.

Belford, G. G., Belford, R. L. and Weber, G. (1972). *Proc. Natl. Acad. Sci. USA* **69**, 1392–0000.

Drake, R., Phillips, D., Roberts, A. J. and Soutar, J. (1982). In "Photophysics of

Synthetic Polymers" (Phillips, D. and Roberts, A. J., eds), pp. 150–160. Science Reviews, Northwood.
Dubois-Violette, E., Geny, F., Monnerie, L. and Parodi, O. (1969). *J. Chem. Phys.* **66**, 1865–1876.
Ghiggino, K. P., Roberts, A. J. and Phillips, D. (1981). *Adv. Polym. Sci.* **40**, 69–167.
Harvey, S. C. and Cheung, H. C. (1972). *Proc. Natl. Acad. Sci. USA* **69**, 3670–3672.
Kinoshita, K., Kawato, S. and Ikegami, A. (1977). *Biophys. J.* **20**, 289–305.
Lipari, G. and Szabo, A. (1980). *Biophys. J.* **30**, 489–506.
Lombardi, J. R. and Dafforn, G. A. (1966). *J. Chem. Phys.* **44**, 3882–3887.
Mielenz, K. D., Cehelink, E. D. and McKenzie, R. L. (1976). *J. Chem. Phys.* **62**, 477–489.
Munro, I., Pecht, I. and Stryer, L. (1979). *Proc. Natl. Acad. Sci. USA* **76**, 56–63.
Small, E. W. and Isenberg, I. (1977). *J. Chem. Phys.* **66**, 3347–3351.
Spencer, R. D. and Weber, G. (1969). *Ann. N.Y. Acad. Sci.* **158**, 361–384.
Spencer, R. D. and Weber, G. (1970). *J. Chem. Phys.* **52**, 1654–1663.
Tao, T. (1969). *Biopolym.* **8**, 609–632.
Tschanz, H. P. and Binkert, Th. (1976). *J. Phys. E* **9**, 1131–1136.
Valeur, B. and Monnerie, L. (1976). *J. Polym. Sci. Polym. Phys.* **14**, 11–40.
Wahl, Ph. (1975). *Chem. Phys.* **7**, 210–219.
Wahl, Ph. (1979). *Biophys. Chem.* **10**, 91–104.
Weber, G. (1971). *J. Chem. Phys.* **55**, 2399–2407.
Williams, G. (1978). *Chem. Soc. Rev.* **7**, 89–131.